Check for updates

Fabrication of PAA-*co*-PNIPAm brushes *via* surface-initiated-PET-RAFT polymerization and investigation of their dual responsive behavior

Asya Eroğlu, Özge Laçin [ID] and Ertan Yildirim [ID] *

Stimuli-responsive polymers have attracted considerable attention because they can alter their chemical structures or physical properties in response to external triggers. Such smart polymers have found applications in various fields, including sensors, drug delivery, water purification, recyclable catalysis, separation, and more. Polymers exhibiting stimuli responsive behavior have been synthesized in response to various stimuli to date. In this study, the relatively new PET-RAFT polymerization technique was employed to synthesize and characterize both homo- and copolymer brushes on silicon disc surfaces. Brushes consisting of a single polymer segment (poly(acrylic acid) (PAA), poly(*N*-isopropylacrylamide) (PNIPAm)) and two polymer segments ((PAA-*co*-PNIPAm), denoted as P1, P2 and P3) were prepared using SI-PET-RAFT polymerization to analyze their stimuli responsive behavior for the first time. Water contact angle (WCA) measurements revealed pH- and temperature-triggered transitions. PAA brushes showed a distinct transition around pH 5–6, with the WCA decreasing by approximately 35° as pH increased from 4 to 6. PNIPAm brushes exhibited a thermal transition near 30 °C, with the WCA increasing by about 10° as the temperature increased from 28 °C to 32 °C. The copolymer brushes displayed composition-dependent tunable responses. P1 (PAA-rich) presented a sharp pH transition around pH 5, with the WCA decreasing by approximately 46° as pH increased from 4 to 6. P2 (equimolar PAA/PNIPAm) showed a slightly less sharp pH transition around pH 5–6, with WCA decreasing by around 39° over pH 4–6. P3 (PNIPAm-rich) exhibited a transition around pH 5, with WCA decreasing by roughly 36° over the same range. Although the sharpness of the pH-induced transition slightly decreased from P1 to P2 and P3 as the PAA fraction decreased and PNIPAm fraction increased, a clear pH response was retained. Thermally, P1 and P2 underwent transitions around 29 °C, with WCA increasing by about 10° and 7.5° respectively, as the temperature increased from 28 °C to 32 °C. P3 showed a slightly shifted transition around 31 °C, with WCA increasing by about 10.5° over the same range. These findings demonstrate that dual responsive behavior can be tuned by monomer composition, thereby offering potential for controlled drug delivery and other bio-related applications.

Introduction

Various external stimuli (temperature, pH, light, *etc.*) are involved in understanding the response processes of polymers and investigating their characteristic behaviors. These stimuli allow the monitoring of changes in many conformational, physical, and chemical processes. In particular, the conformational changes and properties in the basic structures of polymers play an important role in applications such as biosensors, drug purification, and transportation, *etc.* This responsive behavior of polymers enables control over interactions within polymer chains, such as dissolution and precipitation.

In the design of responsive systems, processes influenced by various stimuli can be explored. One of the most studied stimuli

is temperature. In this context, the lower critical solution temperature (LCST) of temperature-sensitive polymers can be determined, and the conformational changes in polymer chains can be interpreted based on the LCST. It is known that at temperatures below the LCST, polymer chains can molecularly dissolve in the solution, resulting in a clear, homogeneous, and expanded structure. Conversely, at temperatures above the LCST, aggregation occurs, causing turbidity and precipitation in the polymer solution. As the temperature of the solution containing the polymer increases, hydrophobic interactions in temperature-sensitive polymer chains enhances.[1] These systems, in which temperature sensitivity is investigated, have the potential to be used in various applications, including drug and gene delivery systems, as well as biomedical fields.[1–9] Another extensively studied stimulus is the pH value. pH-sensitive polymers are known for undergoing conformational changes in their chains, which affect the solubility and spatial

Department of Chemistry, Science Faculty, Gazi University, 06500 Ankara, Turkey.
E-mail: ertan.yildirim@gazi.edu.tr

arrangement depending on solution pH value.[10] For polymer chains containing ionizable groups, changes in physicochemical properties can be observed with changing pH. The proton mobility in polymers containing functional groups such as amino and carboxylic acids, resulting from pH changes, depends on the polymer's pK_a value. Depending on the pH of the medium, the functional groups become protonated or deprotonated. This process affects the dissolution and precipitation/aggregation behavior of polymers. For basic functional groups, at pH values lower than the polymer's pK_a they are protonated, increasing hydrophilicity, while at pH values above the pK_a they become neutral, leading to reduced hydrophilicity.[11,12] In contrast, for acidic functional groups, at pH values lower than the pK_a they remain protonated, making the polymer less hydrophilic, whereas at pH values higher than the pK_a they deprotonate, increasing hydrophilicity. pH-sensitive polymers bearing cationic groups have been studied for extracellular tissue targeting, where the appropriate selection of ion-supplying amine functional groups plays a crucial role due to weak basic nature under neutral pH conditions.[13]

The use of controlled/living radical polymerization (CLRP), also known as reversible-deactivation radical polymerization (RDRP), offers significant benefits, particularly in controlling stimulus responsive processes. These advantages include control of polymer chain length, homogeneous growth, control of kinetic processes, and low molecular weight distribution.[14,15] The presence of activation/deactivation steps in all mechanistic processes of radicals formed in RDRP techniques is crucial for controlling the polymerization process. Furthermore, the dynamic equilibrium between living and dead polymer chains can be controlled by the radicals formed.[16] This also provides insights into the control of conformational processes in polymer chains. The polymerization environment, combined with the control of the process and molecular weight, provides important clues for obtaining different architectures (block, star, and branched, *etc.*).[17] Among RDRP techniques, reversible addition–fragmentation chain transfer (RAFT) polymerization, in particular, eliminates the use of metal catalysts and allows the use of a wide range of monomer types under mild conditions.[18–20] In RAFT polymerization, a living process occurs between the radical source and the polymer chains through degenerative transfer processes.[18] New types of controlled/living radical polymerization, particularly those based on RAFT, have emerged with various mechanisms. In recent years, the need for a process that is sustainable, minimizes environmental pollution and reduces chemical processing has arisen. Photoinduced electron transfer–reversible addition–fragmentation chain transfer (PET-RAFT) polymerization, first reported in 2014, is a light-initiated type of RAFT polymerization and an innovative approach that avoids the use of chemical initiators, enables polymerization through simple mechanisms, and contributes to green chemistry.[21] Over the past decade, this technique has been developed to offer several advantages over other controlled/living radical polymerizations. SI-PET-RAFT method, surface-initiated form of PET-RAFT, enables the direct growth of polymer brushes on surfaces. This method is based on the covalent attachment of a RAFT agent (chain transfer agent, CTA) to a surface, followed by the controlled growth of polymer chains, allowing precise regulation of parameters such as chain length, grafting density, molecular weight distribution, and brush thickness.[22–25] Upon light irradiation, a photocatalyst is excited and generates radicals through electron/energy transfer, and the controlled polymer chain growth occurs *via* a RAFT agent.[22,25] Due to not requiring metal catalysts, exhibiting low toxicity, being compatible with aqueous systems, and operating under low energy demand, it provides a safe polymerization strategy suitable for green chemistry and a broad range of applications, such as surface functional coatings, sensors and biomedical applications.[19,22,26–29] Moreover, its tolerance to oxygen allows polymerization to proceed under ambient air without requiring an inert atmosphere, making the process easier to apply and more cost-effective. The light-initiated polymerization mechanism provides fine control over the reaction, and the broad monomer compatibility enables the achievement of desired properties.[19,22,30]

In the literature, various studies of stimuli-responsive polymers synthesized by CLRP have been conducted. Woods *et al.*, reported the synthesis of temperature-responsive lactic acid-based nanoparticles. *N,N*-dimethyl lactamide acrylate (DMLA) and ethyl lactate acrylate (ELA) monomers were used to prepare diblock copolymer nanoparticles (PDMLA-*b*-PELA) by applying RAFT aqueous emulsion polymerization.[31] These polymer nanoparticles exhibited reversible LCST behavior in water, accompanied by an increase in particle average diameter upon heating.[31] Dual-stimuli responsive polymers, including poly(*N*-acryloyl-L-proline methyl ester) as a thermo-responsive segment, poly(*N*-acryloyl-L-proline) as a pH-responsive segment, was synthesized *via* RAFT polymerization.[32] The response behavior to pH and temperature was investigated with altering pH, salt concentration, and monomer composition, all of which affect LCST, alongside an evaluation of chiroptical properties and assembled structures through circular dichroism and dynamic light scattering measurements.[32] Dual-responsive (temperature and pH) polymers, comprising poly(methacrylic acid) (PMAA), poly(*N,N*-dimethyl aminoethyl methacrylate) (PDMAEMA), and poly(methacrylamide azobenzene) (PMAAAB) blocks, were utilized for controlled demulsification and desorption after their synthesis by RAFT polymerization.[33] Their modifiable amphiphilicity and wettability were investigated using UV-Vis transmittance and contact angle measurements. RAFT polymerization was employed to synthesize temperature-responsive copolymer, incorporating poly(*N*-vinylimidazolium salt) as a poly(ionic liquid) segment, and poly(*N*-isopropylacrylamide) (poly(NIPAm)) as a thermoresponsive segment.[34] Thermally induced phase separation and assembled structures were modified by controlling monomer composition, chain structure, and external stimuli (temperature and salt concentration).[34] pH responsive behavior of triblock copolymer, consisting of α-methoxypoly(ethylene oxide)-*b*-poly[*N*-(3-aminopropyl) methacrylamide]-*b*-poly[2-(diisopropylamino)ethyl methacrylate] (mPEO–PAPMA–PDPAEMA), was analyzed after being synthesized by RAFT polymerization in aqueous media.[35]

At pH values below 5 dissolution occurred because of protonation of amine groups in PAPMA and PDPAEMA. In contrast, at pH above 5 self-assembly into micelles with DPAEMA cores, PAPMA shells, and mPEO coronas was observed.[35] By applying RAFT polymerization in methanol solution, poly(N-isopropylacrylamide)-block-poly(acrylic acid) polymers (PNIPAm-b-PAA) were generated, and their responses to pH and temperature stimuli were investigated.[36] Block copolymers of poly(N-isopropylacrylamide-b-acrylamide) (PNIPAm-b-AM), prepared via PET-RAFT polymerization mediated by zinc porphyrins, exhibited thermo-sensitive properties that could be modified by varying AM content.[37]

Stimulus-responsive PNIPAm in the form of brushes, was prepared on gold coated surfaces in 2004 by using surface initiated atom transfer radical polymerization (ATRP).[38] Conformational height changes were identified, influenced by LCST and solvent type. In another study, PNIPAm brushes were synthesized on functionalized latex particles via ATRP, and their responses to both temperature and salt concentration were examined.[39] A polymer brush mixture, containing poly(N-isopropylacrylamide) (PNIPAm) and poly(methacrylic acid) (PMAA), was fabricated via surface initiated ATRP on gold substrates, and its responsive behavior under different pH was studied.[40]

Polymer brushes synthesized via SI-PET-RAFT method have been reported to exhibit a broad range of functional properties such as antifouling, antibacterial, antiviral, biosensing, semi-conducting, and hydrophobic characteristics.[41–50] Temperature-responsive poly(di(ethylene glycol)methyl ether methacrylate) (PDEGMA) brushes were synthesized on titanium dioxide coated glass surfaces and modified with vancomycin, achieving controlled antibiotic release and significant inhibition of bacterial biofilm formation.[50] Functionalizing the surface of flame-retardant polyester fabrics with poly(glycidyl methacrylate) (PGMA) brushes and benzotriazole produced hydrophobic, anti-UV dual-functional coatings.[46] Polymer brushes synthesized from N-[3-(decyldimethyl)-aminopropyl]methacrylamide bromide and carboxybetaine methacrylamide monomers provided effective antiviral properties.[43] Three different polymer brushes formed from oligo(ethylene glycol) methacrylate, N-(2-hydroxypropyl)methacrylamide, and carboxybetaine methacrylamide demonstrated strong antifouling properties against proteins and complex biological matrices.[41] Thermoresponsive poly(di(ethylene glycol) methyl ether methacrylate) (PMeO$_2$MA) brushes, synthesized by SI-PET-RAFT, enabled temperature-controlled cell adhesion.[51]

To the best of our knowledge, SI-PET-RAFT polymerization of acrylic acid (AA) and N-isopropylacrylamide (NIPAm) to fabricate dual-responsive polymer brush architectures has not been previously reported in the literature. The SI-PET-RAFT method enables controlled surface-initiated polymerization under mild, oxygen-tolerant, and metal-free conditions. Poly(acrylic acid) (PAA) contains ionizable carboxylic acid groups, imparting pH responsiveness through protonation/deprotonation transitions, while poly(N-isopropylacrylamide) (PNIPAm) exhibits a LCST transition, enabling temperature-triggered conformational changes.[10,52–54] The combination of the SI-PET-RAFT polymerization method with these monomers enables the fabrication of polymer brushes with dual pH- and temperature-responsive behavior, providing a surface-grafted, purpose-designed platform for stimuli-responsive functional materials.

In this work, both homo- and copolymer brushes were synthesized on silicon disc surfaces, and the dual-responsive behavior of copolymer brushes was investigated. Brushes consisting of a single polymer segment (PAA, PNIPAm) and two polymer segments (PAA-co-PNIPAm, with varying monomer unit compositions) were prepared using SI-PET-RAFT polymerization to analyze stimuli-responsive behavior. PAA-co-PNIPAm brushes responded to both temperature and pH stimuli, depending on the monomer composition. This property renders them promising candidates for targeted drug delivery and bio-related applications.

Materials and methods

Chemicals and reagents

High purity ethanol (≥99.5%, ACS reagent), acetone (≥99.5%, ACS reagent), tris–HCl (TBS, Tris buffered saline, with Tween™ 20, pH 8.0), dopamine–HCl (≥98% (TLC), powder, neurotransmitter), 2-(dodecylthiocarbonothioylthio)-2-methylpropionic acid (DDMAT, 98% (HPLC)), dichloromethane, DCM (for analysis EMSURE® ACS, ISO, Reag. Ph Eur), acrylic acid, AA (anhydrous, contains 200 ppm MEHQ as inhibitor, 99%), n-isopropyl acrylamide, NIPAm (97%), Eosin Y (dye content ∼99%, powder), triethylamine (suitable for HPLC, LiChropur™, ≥99.5% (GC)), dimethyl formamide, DMF (anhydrous, 99.8%) chemicals were supplied by Sigma-Aldrich. Necessary purification of monomers and stabilizer removal processes were carried out before polymerization. To investigate pH-responsive behavior, the following buffer solutions were used: Britton–Robinson (BR) buffer (pH 3–5), phosphate buffer (pH 6–8), and glycine–HCl–NaOH buffer (pH 9–10).

Activation and characterization of silicon disc surfaces

Silicon disc surfaces were cut into 1 cm^2 × 1 cm^2 dimensions. To remove organic contaminants from the silicon disc surface, they were washed with ethanol and distilled water and dried with nitrogen gas. They were then exposed to a UV–ozone device for 20 minutes to remove organic contaminants from the surface, resulting in hydroxyl-terminated surfaces. Water contact angle measurements were performed to characterize the hydroxyl-terminated surfaces.

Covalent bonding of dopamine molecules to activated silicon disc surfaces

A dopamine molecule containing amine-terminated groups was attached to the surface for PET-RAFT polymerization initiated on the surface. To bind the dopamine molecule to the surface, the activated surfaces were incubated in 1 mL of Tris–HCl (10 Mm pH 8.5) buffer solution containing 2 mg of dopamine HCl at room temperature for 2 hours. The surfaces were then washed again in the same buffer solution to remove any remaining dopamine molecules and physical contaminants.[55]

Surfaces dried with nitrogen gas were characterized using X-ray photoelectron spectroscopy (XPS), water contact angle, attenuated total reflectance-fourier transform infrared spectroscopy (ATR-FTIR), and ellipsometry.

Covalent bonding of 2-(dodecylthiocarbonothio)-2-methylpropionic acid (DDMAT) to dopamine-functionalized surfaces

0.22 g of the N-hydroxysuccinimide-activated DDMAT was weighed and placed into 20 mL of dichloromethane containing dopamine-functionalized surfaces. The reaction mixture was stirred under a nitrogen atmosphere for 20 minutes and left at 50 °C for 48 hours. The surfaces were then washed with ethyl acetate and dichloromethane and dried with nitrogen gas.[56]

Synthesis and characterization of PAA and PNIPAm brushes using the PET-RAFT polymerization technique

DDMAT-bound surfaces were immersed in a polymerization solution containing acrylic acid, Eosin-Y, and triethylamine at specific ratios for poly(acrylic acid) (PAA) and poly(N-isopropylacrylamide) (PNIPAm) synthesis via SI-PET-RAFT polymerization. Characterization was performed to evaluate the conformational structure, chemical composition, and functional group bands of the PAA and PNIPAm brushes, as well as the brush thickness at different polymerization times. To demonstrate the controlled growth of the PAA and PNIPAm brush chains, brush thicknesses and changes in band intensities in ATR-FTIR spectra were determined for samples polymerized for specific periods.

Synthesis of PAA-co-PNIPAm brushes

For SI-PET-RAFT polymerization, copolymers were prepared at three different monomer ratios. For the synthesis of PAA-co-PNIPAm brushes on the silicon disc surfaces that were functionalized through covalent attachment of DDMAT, PET-RAFT components such as Eosin-Y and triethylamine were used in fixed and defined proportions. Polymer brushes were prepared in DMF solvent for various polymerization times for each copolymer sample. The thicknesses of the polymer brushes synthesized at different times were measured using ellipsometry. Water contact angle (WCA) measurements were conducted to evaluate surface functionalities. The presence of functional groups on the surfaces was analyzed by ATR-FTIR spectroscopy. Surface morphology was determined using atomic force microscopy (AFM), and surface chemical composition analysis was performed using XPS techniques.

Investigation of temperature- and pH-responsive behavior of PAA-co-PNIPAm brushes

To investigate the temperature- and pH-responsive behavior of PAA-co-PNIPAm copolymers synthesized via surface-initiated PET-RAFT polymerization at different monomer ratios, water contact angle measurements were conducted at various temperatures and pH values.

Characterization techniques

Attenuated total reflectance-fourier transform infrared (ATR-FTIR) spectra of the synthesized polymer brushes were obtained on a Thermo-Nicolet model 6700 instrument with a scan number of 32 and a resolution of 4 cm^{-1} using the grazing angle module. Water contact angle (WCA) measurements of the polymer brushes were conducted on a Krüss brand ganiometer instrument using DSA 100 software by using distilled water (4 μL, 18 MΩ cm resistivity) on three different regions of the surfaces. Atomic force microscopy (AFM) images of the surfaces (3 mm × 3 mm) were taken using a Park Systems XE70 SPM Controller LSF-100 HS Multimode Atomic Force Microscope (AFM). Ellipsometric measurements of the surfaces were performed using the DRE, EL X20C branded ellipsometer and the He–Ne Laser (632.8 nm). X-ray photoelectron spectroscopy (XPS) analyses were carried out using SPECS brand Flex mode system.

Results and discussions

Covalent bonding of dopamine molecules to activated silicon disc surfaces

In surface-initiated PET-RAFT polymerization, various intermediate molecules are preferred for facilitating the conjugation of the RAFT agent to the surface. In particular, intermediate linker molecules containing amine-, hydroxyl-, or other functional group-terminated are used in the conjugation of the RAFT agent.[57] The covalent binding of these intermediate linker molecules to the surface affects the RAFT agent concentration bound to the surface. Changing the RAFT agent concentration plays an important role in the steric effect and binding density of the polymer brushes on the surface. The presence of molecules with active end groups present on the surface increases the binding density of polymer brushes.

In this study, dopamine molecules with amine groups were covalently bound to the surface as intermediate linkers. ATR-FTIR, XPS, AFM, WCA, and ellipsometry were used to characterize dopamine-bound surfaces.

In the ATR-FTIR spectrum taken from the surface, the functional bands due to aromatic O–H stretching vibration, aromatic C=C stretching vibration, and N–H vibration, specific to dopamine, were detected at approximately 3426 cm^{-1}, 1626 cm^{-1} and 1516 cm^{-1} respectively (Fig. 1a).[58] The XPS survey spectrum obtained from the surface revealed the peaks corresponding to C 1s, O 1s, and N 1s atoms of dopamine at 285.3, 532.1, and 400.6 eV, respectively (Fig. 1c). The experimental N/C ratio in Si-PDA was 0.95 ± 0.01, which is close to the theoretical value for the dopamine molecule (0.125).[59] The %N, %C, and %O values determined by XPS were close to theoretical values. In the high-resolution XPS spectrum of N 1s atom, three nitrogen bonding states with distinct chemical environments were identified at 398.6 eV (N=C), 400.3 eV (C–NH–C), and 401.6 eV (H$_2$N–C) (Fig. 1b).[59] Regarding the surface morphology, partial islands were formed in the AFM image, and the rms value, which is the surface roughness measurement, was found to be 0.35 ± 0.12 (Fig. 1d). The WCA result, which relates to the chemical composition of the surface originating from the
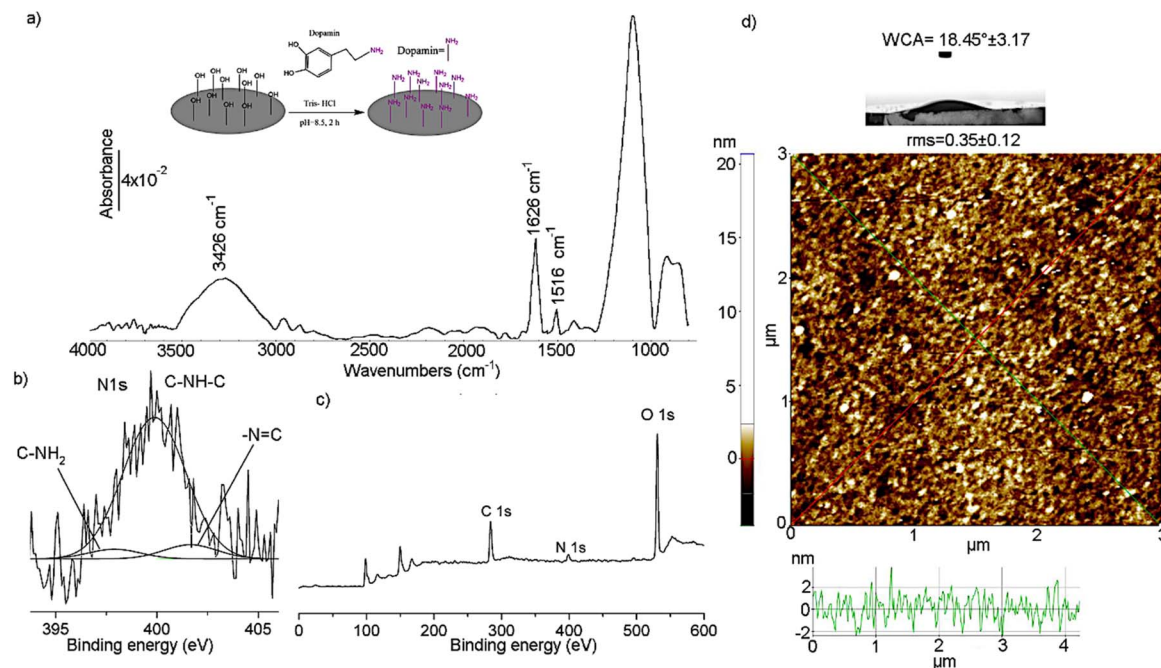
Fig. 1 (a) ATR–FTIR spectrum of the dopamine-functionalized surface (b) high-resolution XPS spectrum of N 1s for the dopamine-functionalized surface (c) XPS survey spectrum of the dopamine-functionalized surface (d) 2D-AFM and WCA measurement images of the dopamine-functionalized surface (top: schematic representation of dopamin functionalization of the surface).

dopamine, was determined to be approximately 18.45° ± 3.17 (Fig. 1d).[58] The small WCA value was attributed to the interaction of the amine groups in the dopamine molecule with water molecules, which confers hydrophilic properties on the surface. The film thickness of dopamine-bound surfaces was measured as 10 nm by ellipsometer.[60] All these results and characterization analyses indicate that the dopamine molecule is covalently attached to the surface.

Covalent bonding of 2-(dodecylthiocarbonothio)-2-methylpropionic acid (DDMAT) to dopamine-functionalized surfaces

For surface-initiated PET-RAFT polymerization, the concentration and type of RAFT agent on the surface affect several parameters including bond density, uniform chain length, polymerization control, and polymerization rate. The RAFT agent covalently bound to the surface was selected based on AA and NIPAm monomers. The trithiocarbonate type RAFT agent DDMAT has been reported to be compatible with both acrylate monomers (acrylic acid (AA)) and acrylamide monomers (*N*-isopropylacrylamide (NIPAm)) in various studies, as also indicated in the Sigma Aldrich RAFT agent to monomer compatibility table.[37,47,61,62] The NHS-activated form of DDMAT was covalently attached to the surface by amide bonding without any additional chemical processing. Converting the carboxylic acid group of the RAFT agent into its *N*-hydroxysuccinimide (NHS) ester makes this group significantly more reactive. Such NHS-ester derivatives of RAFT agents readily and efficiently react with surface amine groups, enabling fast and high-yield covalent attachment through stable amide bond formation.[25]

The presence of DDMAT on the surface was confirmed by using ATR-FTIR for functional group analysis, XPS for elemental composition, AFM for surface morphology, water contact angle measurements for surface composition, and ellipsometry for film thickness determination.

In the ATR-FTIR spectrum obtained from the surface, the functional group bands specific to DDMAT were detected at approximately 2950–3030 cm^{-1} (aliphatic bands), 1720 cm^{-1} (C=O), and 1600 cm^{-1} (C=S) (Fig. 2a).[63] The high resolution XPS spectrum of S 2p region on the surface indicated two sulfur bonding states with different chemical environments, identified at 165.4 eV (S=C), and 167.6 eV (S–C) (Fig. 2b).[63] The XPS survey spectrum showed the peaks attributed to S, C, N and O atoms, present in DDMAT, at 161.2, 285.3, 400.6 and 532.1 eV, respectively (Fig. 2c). The %S, %N, %C, and %O values determined from XPS were close to theoretical values. The surface rms value increased compared to the dopamine-functionalized surface, reaching 0.51 ± 0.13, which led to more visible surface islands according to the AFM analysis (Fig. 2d). At the same time, the introduction of DDMAT, which contains more aliphatic groups than dopamine, altered the surface composition, increasing the water contact angle from 18.45° ± 3.17 to 77.89° ± 4.58 (Fig. 2d).[63] The surface film thickness also increased by approximately 3 nm, reaching to 13.47 ± 1.56 nm. The characterization results indicated the covalent bonding of the DDMAT molecule to the surface.

Synthesis of PAA-*co*-PNIPAm brushes

Morphological, physical, and chemical processes in polymeric structures, influenced by various stimuli (temperature, pH, ionic
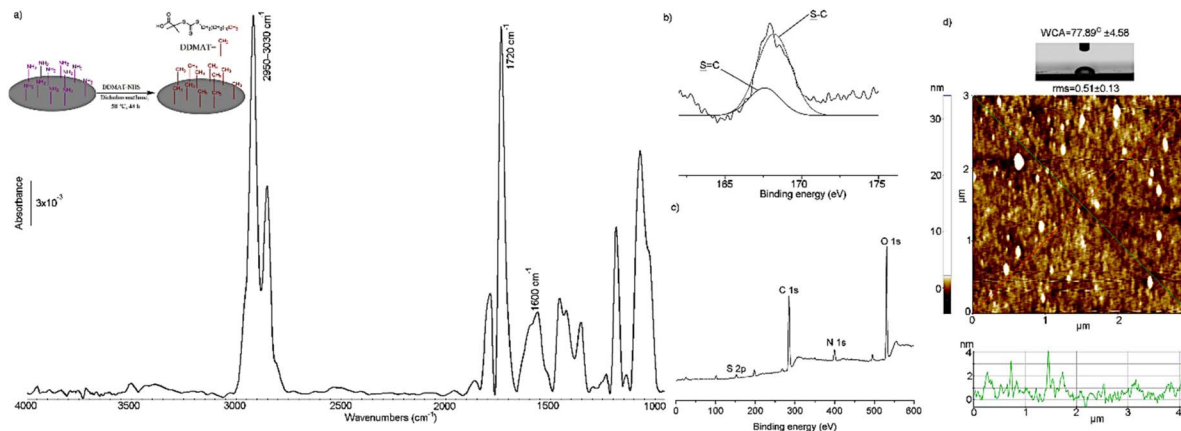
Fig. 2 (a) ATR-FTIR spectrum of the DDMAT-bound surface (b) high-resolution XPS spectrum of S 2p for the DDMAT-bound surface (c) XPS survey spectrum of the DDMAT-bound surface (d) 2D-AFM and WCA measurement images of the DDMAT-bound surface (top: schematic representation of DDMAT attachment to the surface).
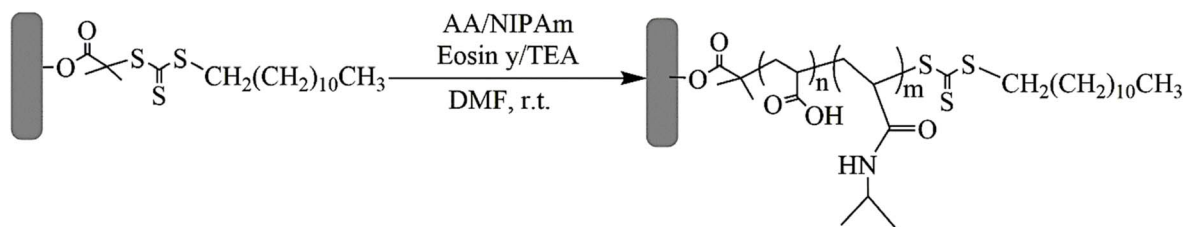

Fig. 3 Schematic representation of the PAA-*co*-PNIPAm brush synthesis *via* SI-PET-RAFT polymerization.

strength, *etc.*), have been widely studied. Systematic approaches have been employed to analyze these processes in polymer systems. Specifically, to determine a single effect, monomeric units sensitive to a single effect are selected, while to determine the processes of multiple effects, information is obtained from copolymeric structures. Some copolymeric structures have been subject to investigations of the effects such as temperature-pH, temperature-salt, temperature-light, or pH-ionic strength. In this study, a pH-sensitive AA monomer and a temperature-sensitive NIPAm monomer were chosen as model compounds to investigate pH- and temperature-responsive behaviors. PAA, PNIPAm homopolymer brushes, PAA-*co*-PNIPAm copolymer brushes (Fig. 3) were synthesized, and their characterization was performed.

pH-sensitive PAA brushes were used to investigate the stimuli-responsive process. PAA has been frequently studied in the literature because of its non-toxic, biocompatible, readily ionizable, hydrophilic nature, as well as its applicability across diverse fields, especially in drug delivery systems.[64] PAA brushes, which synthesized by using various polymerization techniques in the literature, were synthesized using surface-initiated PET-RAFT polymerization on the silicon disc surfaces in this study. ATR-FTIR, XPS, ellipsometry, AFM, and WCA measurements were performed to characterize PAA brushes. The ATR-FTIR spectra, taken from the surfaces, showed $-C{=}O$ stretching vibration at approximately 1733 and 1650 cm^{-1}, $-CH_2$ bands at 2900–3000 cm^{-1}, and broad $-OH$ bands at 3000–3600 cm^{-1}, which are characteristic

to PAA. Additionally, the intensity of the $-CH_2$, $-OH$ and $-C{=}O$ bands increased linearly with polymerization time (Fig. 4a). The AFM image clearly showed that the polymer brushes formed islands on the surface. The rms value, a measure of surface roughness, was found to be 2.56 ± 0.42 nm after 6 hours of polymerization (Fig. 4b). In the XPS survey spectrum of the PAA brushes, the binding energy peaks for S, C and O atoms, present in PAA, were identified at 161.5 eV, 285.0 eV, and 532.0 eV, respectively (Fig. 4c). Moreover, the brush thicknesses measured from the surfaces after different polymerization times (from 1 h to 6 h) increased linearly (Fig. 4d). In addition to the linear increase in the ATR-FTIR band intensities, the linear increase in the brush thickness indicated successful time-dependent growth of the polymer brushes, *i.e.*, controlled polymerization, during the SI-PET-RAFT process. To demonstrate the pH sensitivity of PAA, WCA measurements were conducted after immersion in buffer solutions of different pH values. According to WCA measurements (Fig. 4e), a distinct pH-triggered transition was observed for the PAA brushes around pH 5–6, which is close to the reported pK_a of PAA (≈ 4.5–5). WCA decreased by $\sim 35°$ (from $\sim 62°$ to $\sim 27°$) as the pH increased from 4 to 6, reflecting strong protonation–deprotonation driven transition. At pH below 5, polymer brushes collapsed and precipitated due to their protonated form, leading to a more hydrophobic surface. At pH above 5, they gradually expanded and dissolved in the deprotonated form, resulting in a more hydrophilic surface.[65]
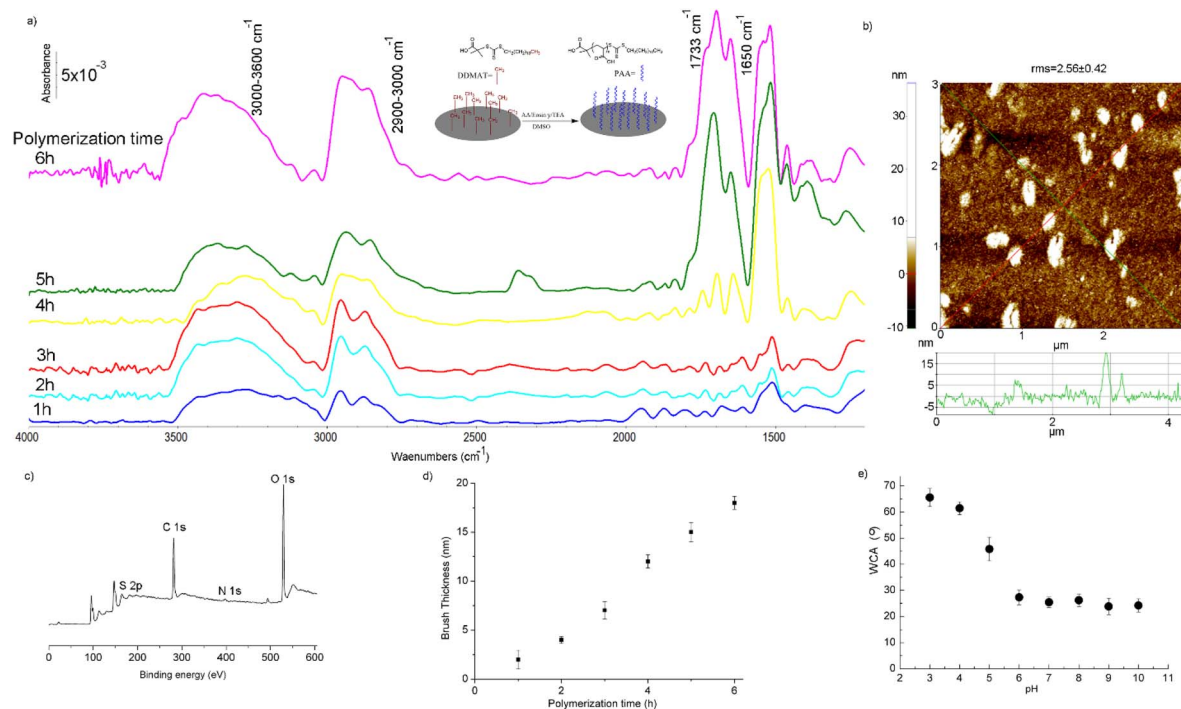
Fig. 4 (a) ATR-FTIR spectra of the PAA brush surface obtained after different polymerization times (1 h to 6 h), labelled on each spectrum. (b) 2D-AFM image of the PAA brush surface after 6 hours of polymerization (polymer thickness ≈18 nm). (c) XPS survey spectrum of the PAA brush surface after 6 hours of polymerization (polymer thickness ≈18 nm). (d) Variation of brush thickness with polymerization time for the PAA brush surface. (e) Variation of WCA measurements with pH for the PAA brush surface (top center: schematic representation of the PAA brush synthesis).
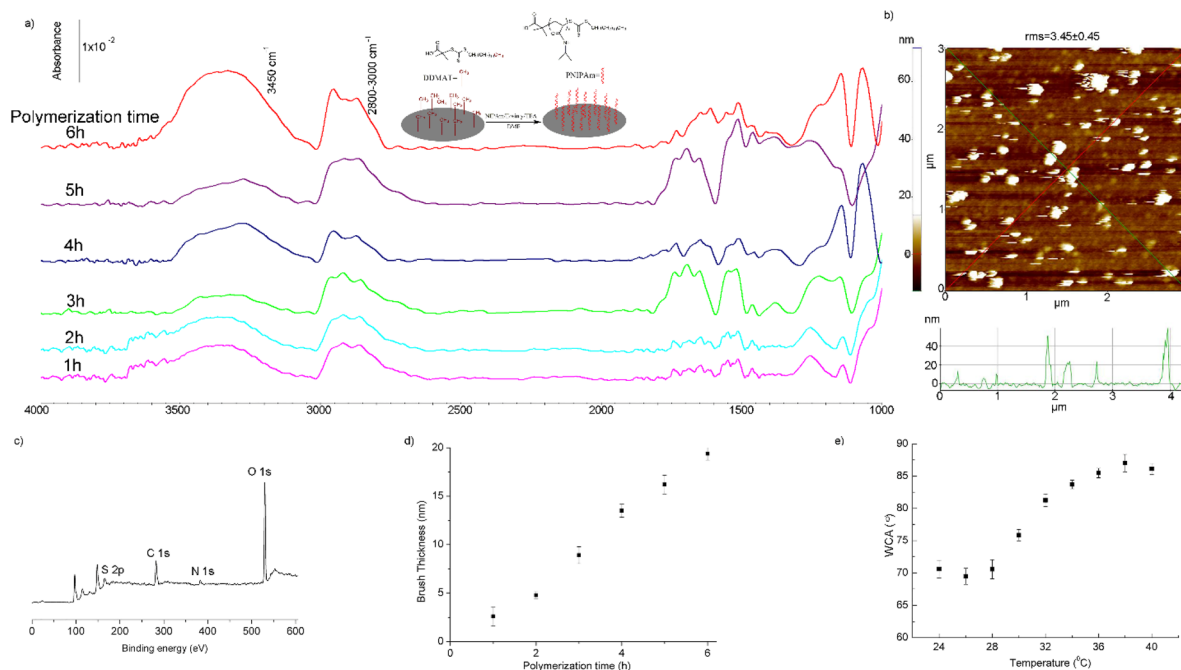

Fig. 5 (a) ATR-FTIR spectra of the PNIPAm brush surface obtained after different polymerization times (1 h to 6 h), labelled on each spectrum. (b) 2D-AFM image of the PNIPAm brush surface after 6 hours of polymerization (polymer thickness ≈19 nm). (c) XPS survey spectrum of the PNIPAm brush surface after 6 hours of polymerization (polymer thickness ≈19 nm). (d) Variation of brush thickness with polymerization time for the PNIPAm brush surface. (e) Variation of WCA measurements with temperature for the PNIPAm brush surface (top center: schematic representation of the PNIPAm brush synthesis).

Thus, the increase in the ATR-FTIR band intensities and brush thickness with polymerization time confirmed the controlled SI-PET-RAFT polymerization (Fig. S1). XPS and AFM analyses further verified successful surface functionalization and the formation of polymer brush islands. WCA measurements demonstrated pH sensitivity of PAA (transition around pH 5–6). Altogether, these results support the suitability of the SI-PET-RAFT method for preparing polymer brushes.

Many temperature-sensitive, water-soluble polymers exhibit lower critical solution temperature (LCST) behavior. In such cases, a temperature-sensitive polymer solution is clear and homogeneous below the LCST due to molecular dissolution of the polymer chains, whereas above the LCST, the solution becomes turbid as a result of chain aggregation and decreased water solubility. The increase in solution temperature enhances hydrophobic interactions between polymer chains.[1] This "smart" response of certain polymers makes them potential candidates in biomedical fields, including drug and gene delivery.[1-9] Among these candidates, PNIPAm has been widely used in various applications, especially in bioapplications, due to its relatively low LCST. In this regard, PNIPAm has been synthesized by different polymerization techniques for numerous applications. In this study, it was synthesized using the surface-initiated PET-RAFT polymerization technique on silicon disc surfaces. ATR-FTIR, XPS, ellipsometry, AFM, and WCA measurements were performed to characterize PNIPAm brushes. The ATR-FTIR spectra, taken from the surfaces, showed –NH (3450 cm^{-1}) and –CH$_2$ ($2850–3000 \text{ cm}^{-1}$) bands, specific to PNIPAm. Moreover, the intensity of the bands increased linearly with polymerization time (Fig. 5a). The AFM image, used to examine the surface morphology, clearly indicated that the polymer brushes formed islands on the surface. The rms value, a measure of surface roughness, was found to be 3.45 ± 0.45 after 6 hours of polymerization (Fig. 5b). In the XPS survey spectrum of the PNIPAm brushes, the binding energy peaks for S, C, N and O atoms were observed at 161.0 eV, 285.0 eV, 400.0 eV, and 532.0 eV, respectively. Particularly, the peak intensity of N atoms in PNIPAm was higher than that observed in the PAA brush surface (Fig. 5c). At the same time, the brush thicknesses recorded from the surfaces after different polymerization times (from 1 h to 6 h) increased linearly (Fig. 5d).

In addition to the linear increase in the ATR-FTIR band intensities, the increase in the brush thickness with polymerization time confirmed that the polymerization was well-controlled during the SI-PET-RAFT process (Fig. S1). To analyze the temperature-sensitivity of PNIPAm, WCA measurements were taken after exposure at different temperatures. According to WCA measurements, as shown in Fig. 5e, the PNIPAm brushes exhibited a clear thermal transition around 30 °C, which corresponds to their lower critical solution temperature (LCST). WCA increased by ∼10° (from ∼71° to ∼81°) as the temperature rose from 28 °C to 32 °C. At temperatures above 30 °C, polymer brushes aggregated and collapsed, leading to a more hydrophobic surface. At temperatures below 30 °C, they extended and hydrated, resulting in a more hydrophilic surface. According to these findings, surface-initiated PET-RAFT polymerization was confirmed to be well-controlled, and PNIPAm brush exhibited temperature-sensitivity.

Table 1 Monomer compositions for P1, P2 and P3

Copolymer name	AA (mmol)	NIPAm (mmol)
P1	5	1.5
P2	5	5
P3	1.5	5

Three different copolymers were synthesized to investigate their response behavior to changes in pH and temperature. The monomer ratios of these copolymers are presented in Table 1. The copolymers were designated as P1, P2, and P3. Detailed characterization of each copolymer was performed sequentially.

ATR-FTIR, XPS, AFM, ellipsometry and WCA measurements were used in the characterization processes for P1 copolymer synthesized by SI-PET-RAFT polymerization. In this regard, the ATR-FTIR spectra obtained from the surface exhibited amide, hydroxyl, and aliphatic bands specific to PAA-co-PNIPAm, with their intensities increased linearly over the polymerization time (Fig. 6a and S1). The brush thicknesses measured from the surfaces after different polymerization times (from 1 h to 6 h) increased linearly (Fig. 6b). In the XPS survey spectrum of the PAA-co-PNIPAm brushes, N, S, O, and C atoms, present in PAA-co-PNIPAm, were detected. Particularly, the peak intensity of N atoms in PAA-co-PNIPAm was significantly lower than that in PNIPAm (Fig. 6c). The AFM image revealed islands formed on the surface, and the rms value reached 3.79 ± 0.67 nm after 6 hours of polymerization (Fig. 6d). The results demonstrated that the copolymer brush was synthesized, and that the polymerization was well-controlled.

The characterization analyses for the P2 copolymer were conducted using the same techniques as those used for the P1 copolymer. The ATR-FTIR spectra showed amide, hydroxyl, and aliphatic bands characteristic of the copolymer, and the intensities of the bands increased linearly with the polymerization time (Fig. 7a and S1). The brush thicknesses measured from the surfaces after different polymerization times (from 1 h to 6 h) increased linearly (Fig. 7b). The XPS survey spectrum of the P2 brush, revealed peaks corresponding to the N, S, O, and C atoms. Notably, the peak intensity of N atoms in P2 was lower than that in PNIPAm, to the point of being barely detectable (Fig. 7c). Islands formed on the surface were observed in the AFM image, and the rms value was found to be 3.19 ± 0.85 nm after 6 hours of polymerization (Fig. 7d). The results confirmed the copolymer brush synthesis and controlled polymerization.

The characterization analyses for the P3 copolymer were carried out using the same techniques as those used for the P1 and P2 copolymers. Bands corresponding to amide, hydroxyl, and aliphatic groups specific to PAA-co-PNIPAm were detected in the ATR-FTIR spectra, showing a linear increase in intensity over the polymerization time (Fig. 8a and S1). At the same time, the brush thicknesses measured from the surface after different polymerization times (1 h and 6 h) increased linearly (Fig. 8b). The XPS survey spectrum of the P3 brush, exhibited peaks corresponding to the N, S, O, and C atoms. Especially, the peak intensity of N atoms in P3 was lower than that in PNIPAm
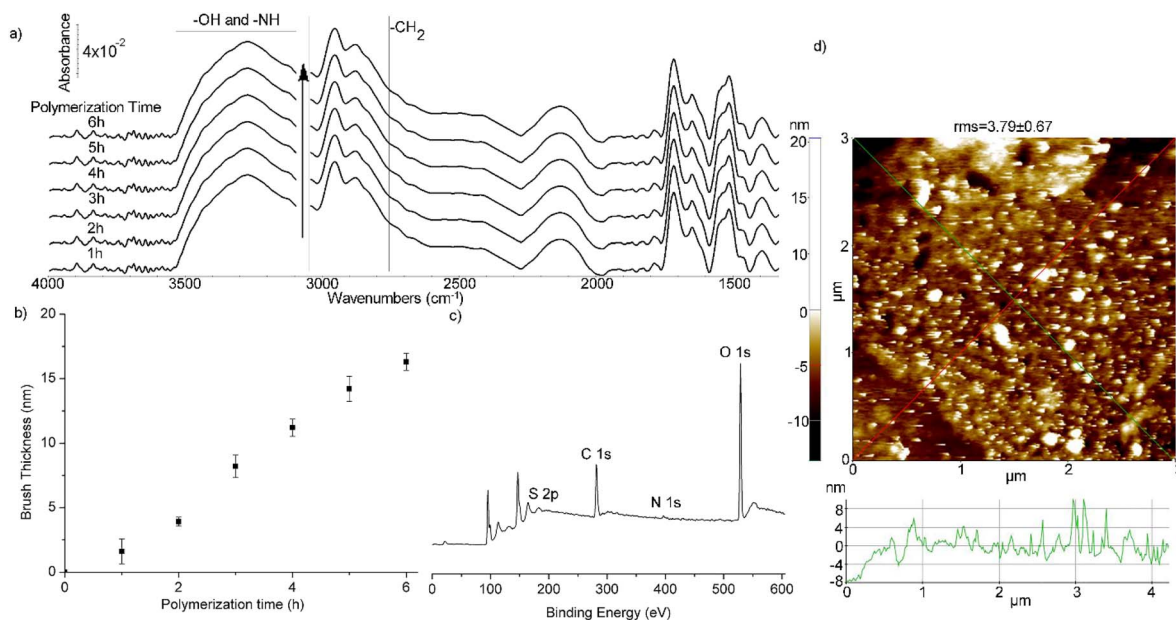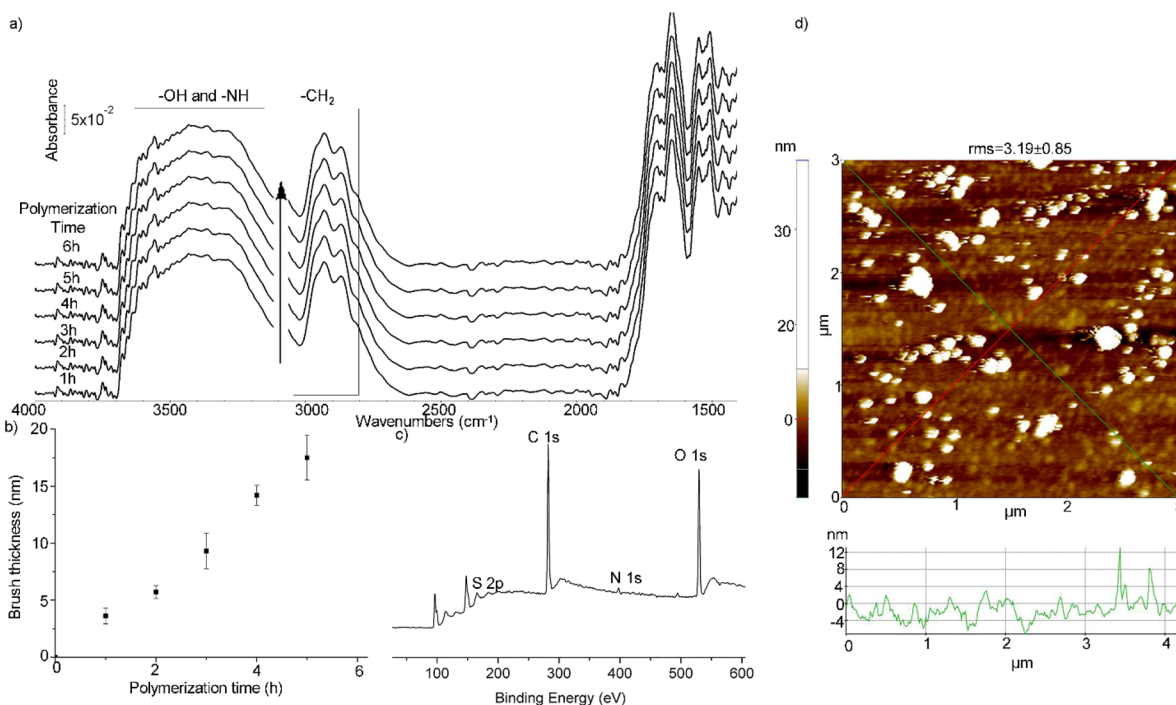
Fig. 6 (a) ATR-FTIR spectra of the P1 brush surface obtained after different polymerization times (1 h to 6 h), labelled on each spectrum. (b) Variation of brush thickness with polymerization time for the P1 brush surface. (c) XPS survey spectrum of the P1 brush surface after 6 hours of polymerization (polymer thickness ≈16 nm). (d) 2D-AFM image of the P1 brush surface after 6 hours of polymerization (polymer thickness ≈16 nm).

Fig. 7 (a) ATR-FTIR spectra of the P2 brush surface obtained after different polymerization times (1 h to 6 h), labelled on each spectrum. (b) Variation of brush thickness with polymerization time for the P2 brush surface. (c) XPS survey spectrum of the P2 brush surface after 6 hours of polymerization (polymer thickness ≈17.5 nm). (d) 2D-AFM image of the P2 brush surface after 6 hours of polymerization (polymer thickness ≈17.5 nm).

(Fig. 8c). The AFM image, used to examine the surface morphology, clearly showed that the polymer brushes formed islands on the surface. The rms value, a measure of surface roughness, was found to be 3.15 ± 0.37 nm after 6 hours of polymerization (Fig. 8d). The results indicated the copolymer brush synthesis and well-controlled polymerization.
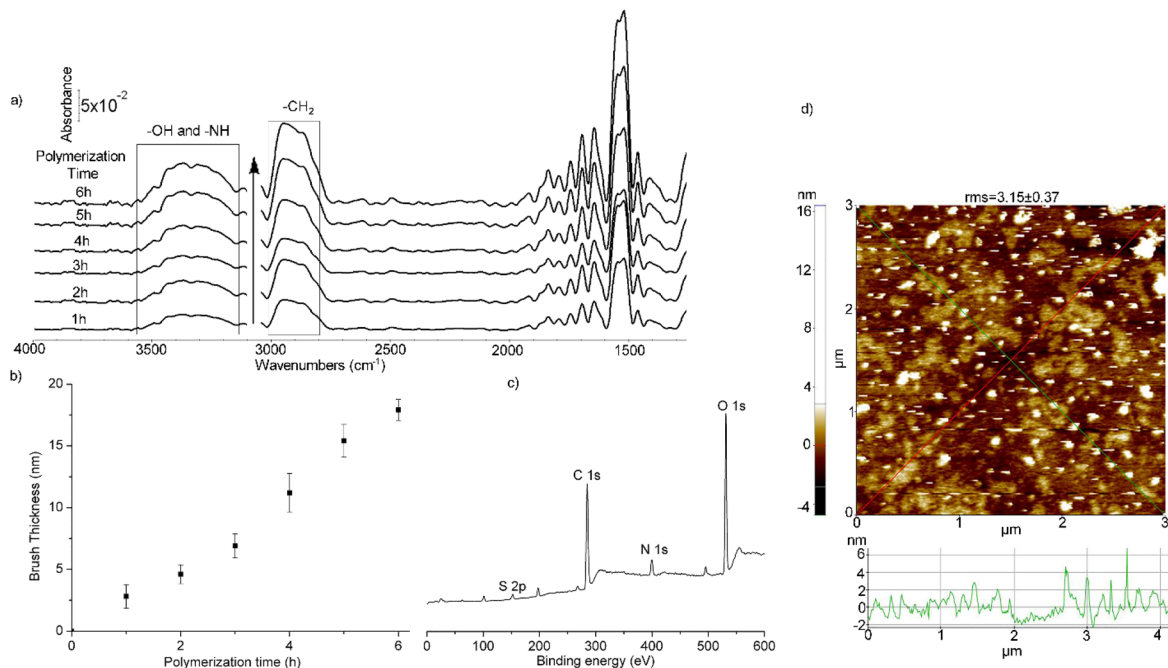
Fig. 8 (a) ATR–FTIR spectra of the P3 brush surface obtained after different polymerization times (1 h to 6 h), labelled on each spectrum. (b) Variation of brush thickness with polymerization time for the P3 brush surface. (c) XPS survey spectrum of the P3 brush surface after 6 hours of polymerization (polymer thickness ≈18 nm). (d) 2D-AFM image of the P3 brush surface after 6 hours of polymerization (polymer thickness ≈18 nm).

In addition to the discussion of the individual characterization of each brush mentioned above, a comparative evaluation of the final brush thickness and surface roughness was performed to provide an overall understanding of the differences among the polymer brushes. After 6 hours of polymerization, ellipsometry measurements showed thicknesses of approximately 18 nm for PAA, ~19 nm for PNIPAm, ~16 nm for P1, ~17.5 nm for P2, and ~18 nm for P3. These results indicate that all homo- and copolymer brushes reached comparable final thicknesses under identical SI-PET-RAFT polymerization conditions, confirming the controlled growth regardless of the monomer feed ratio. The small differences (≤3 nm) among the copolymers can be attributed to intrinsic variations in monomer reactivity and chain density. AFM measurements obtained from representative local regions of each surface revealed rms roughness values of ~2.56 nm for PAA, ~3.45 nm for PNIPAm, ~3.79 nm for P1, ~3.19 nm for P2, and ~3.15 nm for P3. These small variations indicate minor differences in surface topography among the polymer brushes, likely arising from different chain conformations induced by the monomer ratio and the localized nature of AFM imaging.

The dual-responsive behavior of P1, P2, and P3 copolymers, prepared with different monomer ratios, was assessed by WCA measurements under varying pH and temperature conditions. WCA measurements at different pH values, taken at room temperature for P1, P2, and P3 copolymers, are shown in Fig. 9a. P1 (PAA-rich) brushes exhibited a sharp pH-triggered phase transition (dissolution-collapse process) around pH 5, with the WCA decreasing from ~65° at pH 4 to ~19° at pH 6 (ΔWCA ≈

46°). For the P2 brushes (equimolar PAA/PNIPAm), the pH-induced transition became slightly less sharp, occurring around pH 5–6, and the WCA decreased from ~74° at pH 4 to ~35° at pH 6 (ΔWCA ≈ 39°). P3 (PNIPAm-rich) brushes also showed a pH transition around pH 5, but with a lower amplitude, as the WCA dropped from ~78° at pH 4 to ~42° at pH 6 (ΔWCA ≈ 36°). The sharpest transition of P1 demonstrates the dominant effect of the PAA segments, whereas the gradual reduction in ΔWCA from P1 to P2 and P3 indicates the combined modulation of the pH response through PNIPAm incorporation. Although the sharpness of the pH-induced transition slightly decreased from P1 to P2 and P3 as the PAA fraction decreased and PNIPAm fraction increased, a clear pH response was retained.

WCA measurements at pH 7 under varying temperatures are shown in Fig. 9b. P1 and P2 exhibited a transition around 29 °C, with WCA increasing from ~64° to ~74° (ΔWCA ≈ 10°) for P1 and from ~68° to ~75.5° (ΔWCA ≈ 7.5°) for P2 as temperature rose from 28 °C to 32 °C. P3 showed a slightly shifted transition around 31 °C with an increase in WCA from ~71° to ~81.5° (ΔWCA ≈ 10.5°). These results indicate that increasing PNIPAm content slightly shifts the thermal transition toward higher temperatures and can modulate its clarity. P1 retains the clear thermal response despite being PAA-rich, P2 shows the slightly reduced thermal response, while P3 exhibits the thermal transition at the slightly higher temperature, with improved thermal responsiveness due to its PNIPAm-rich composition. Compared to the homopolymers, P1 shows a more pronounced and sharper pH transition than pure PAA (ΔWCA ≈ 35° for PAA),
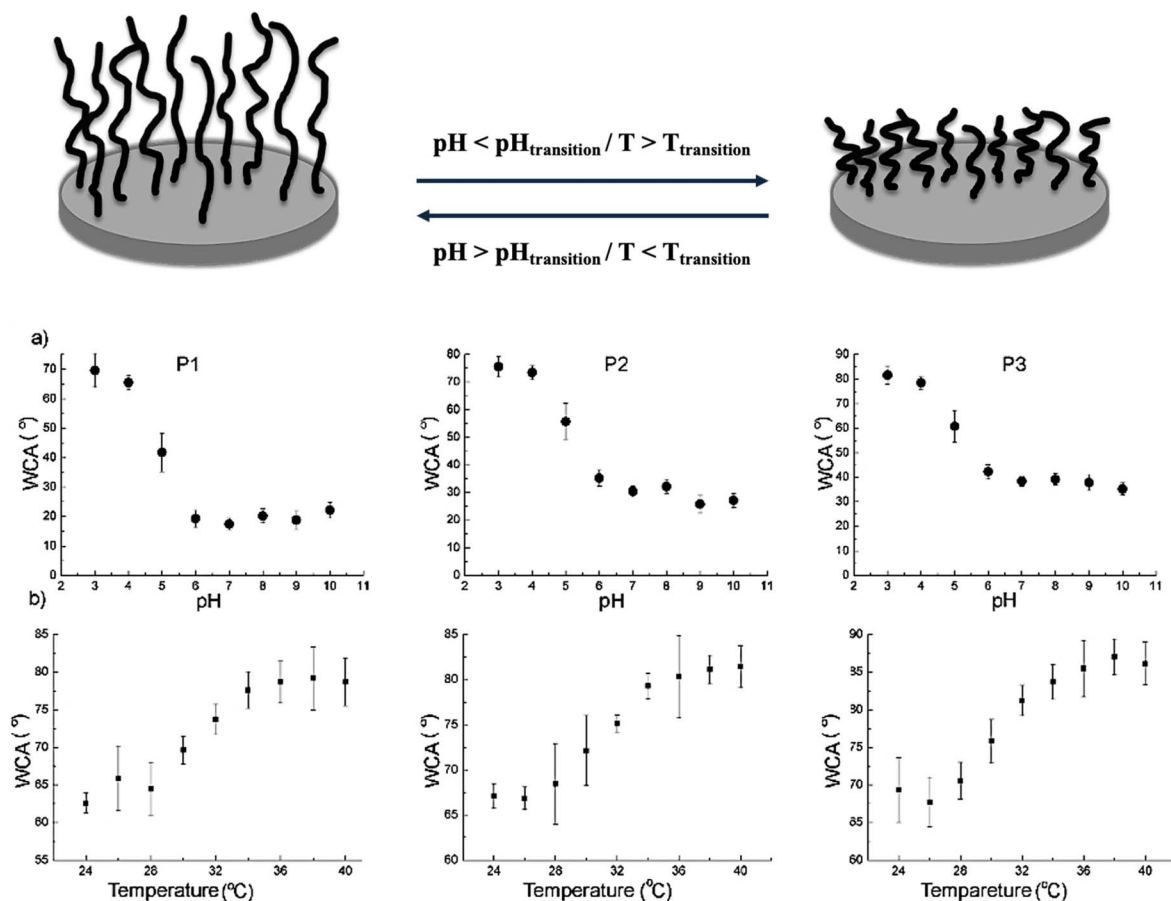
Fig. 9 Variation of WCA measurements for the P1, P2, and P3 copolymers, prepared by SI–PET-RAFT polymerization, with different pH values (a) and with different temperatures (b) (top: schematic representation showing the dual-responsive behavior of the PAA-*co*-PNIPAm brushes on the silicon disk surface under pH and temperature variations).

while P2 and P3 display pH transition sharpness comparable to PAA. All three copolymers maintain a PNIPAm-like thermal transition (ΔWCA $\approx 10°$ for PNIPAm).

Thus, the results demonstrate that the pH responsiveness is primarily governed by the PAA fraction, while thermal responsiveness is dominated by the PNIPAm content. Increasing PNIPAm content slightly reduces but still preserves the pH sensitivity and sharpens the thermal transition, leading to a slight upward shift in transition temperature. Increasing the PAA content strongly enhances and sharpens the pH transition, while slightly suppressing the clarity of the thermal response. P1 provides strong pH responsiveness while retaining a clear thermal response. P3 offers a pronounced thermal response with reduced but still evident pH sensitivity. P2 gives a more balanced, moderate dual response, making it a versatile choice when a well-balanced dual responsiveness is desired.

This composition-dependent tunability shows that SI-PET-RAFT technique enables the rational design of brush surfaces tailored to the dominant stimulus required: P1 for pH-dominated yet thermally active systems, P3 for thermal-dominated applications with some pH sensitivity, and P2 for balanced dual-responsive systems. Furthermore, the composition-dependent transitions arising from the collapse

and dissolution processes of the polymer brushes, which underlie stimuli responsive behaviors, were elucidated, providing valuable insights into the mechanisms governing their dual responsiveness.

Conclusions

In this study, the fabrication, characterization of the homo- and copolymer brushes, as well as the dual-responsive behavior of the copolymer brushes, were investigated. The brushes composed of a single polymer segment (PAA or PNIPAm) and copolymer brushes composed of two polymer segments (PAA-*co*-PNIPAm, with varying monomer unit compositions) were synthesized *via* SI-PET-RAFT polymerization to elucidate their stimuli responsive behavior. Controlled polymerization was confirmed through kinetic analyses. WCA measurements performed at different pH values and temperatures confirmed the pH-responsiveness of PAA, the temperature-responsiveness of PNIPAm, and the combined temperature and pH-responsiveness of the PAA-*co*-PNIPAm brushes. PAA brushes exhibited a sharp pH transition around pH 5–6, while PNIPAm brushes displayed a thermal transition near 30 °C. The copolymer brushes showed tunable dual responsiveness. P1 (PAA-

rich) exhibited strong pH sensitivity and also retained a clear thermal response, with transitions around pH 5 and 29 °C. P2 (equimolar PAA/PNIPAm) maintained both pH and thermal sensitivity but with slightly reduced transition sharpness, showing transitions around pH 5–6 and 29 °C. P3 (PNIPAm-rich) showed strong thermal transition with a moderated yet still evident pH response, with transitions around pH 5 and 31 °C. These findings demonstrate that P1 is the most suitable when strong pH responsiveness is critical while maintaining a significant thermal response; P3 is preferable when a pronounced thermal response is desired with reduced but still evident pH sensitivity; and P2 offers a balanced dual response, providing moderate pH and thermal sensitivity without strongly favoring either trigger, making it a suitable choice for applications requiring a well-balanced dual responsiveness. This composition dependent tunability provides a rational design pathway for designing polymer brush surfaces, offering potential for various applications such as controlled drug delivery and responsive surfaces requiring pH and temperature responsiveness.

Conflicts of interest

There are no conflicts to declare.

Data availability

Additional data are available from the authors upon request.

All data supporting the findings of this article are included in the main text or the supplementary information (SI). Supplementary information is available. See DOI: https://doi.org/10.1039/d5ra06000a.

Acknowledgements

References

1 Y. Kotsuchibashi, M. Ebara, T. Aoyagi and R. Narain, *Polymers*, 2016, **8**, 380.

2 Y. Li, J. Gao, C. Zhang, Z. Cao, D. Cheng, J. Liu and X. Shuai, in *Polymeric Gene Delivery Systems*, ed. Y. Cheng, Springer International Publishing, Cham, 2018, pp. 167–215, DOI: 10.1007/978-3-319-77866-2_7.

3 D. W. Pack, A. S. Hoffman, S. Pun and P. S. Stayton, *Nat. Rev. Drug Discovery*, 2005, **4**, 581–593.

4 Z. Liu, Z. Zhang, C. Zhou and Y. Jiao, *Prog. Polym. Sci.*, 2010, **35**, 1144–1162.

5 V. P. Torchilin, *Pharm. Res.*, 2007, **24**, 1–16.

6 T. G. Park, J. H. Jeong and S. W. Kim, *Adv. Drug Delivery Rev.*, 2006, **58**, 467–486.

7 J. H. Jeong, S. W. Kim and T. G. Park, *Prog. Polym. Sci.*, 2007, **32**, 1239–1274.

8 L. Klouda and A. G. Mikos, *Eur. J. Pharm. Biopharm.*, 2008, **68**, 34–45.

9 J. P. Vacanti and R. Langer, *Lancet*, 1999, **354**, S32–S34.

10 G. Kocak, C. Tuncer and V. Bütün, *Polym. Chem.*, 2017, **8**, 144–176.

11 S. Fujii, E. Mouri, K. Akiyama, S. Nakayama, K. Uda, Y. Nakamura and H. Matsuoka, *Langmuir*, 2017, **33**, 1451–1459.

12 Z. Song, K. Wang, C. Gao, S. Wang and W. Zhang, *Macromolecules*, 2016, **49**, 162–171.

13 K. M. Huh, H. C. Kang, Y. J. Lee and Y. H. Bae, *Macromol. Res.*, 2012, **20**, 224–233.

14 W. A. Braunecker and K. Matyjaszewski, *Prog. Polym. Sci.*, 2007, **32**, 93–146.

15 G. Moad, *Polym. Chem.*, 2017, **8**, 177–219.

16 A. Goto and T. Fukuda, *Prog. Polym. Sci.*, 2004, **29**, 329–385.

17 A. Gregory and M. H. Stenzel, *Prog. Polym. Sci.*, 2012, **37**, 38–105.

18 S. Perrier, *Macromolecules*, 2017, **50**, 7433–7447.

19 Y. Lee, C. Boyer and M. S. Kwon, *Chem. Soc. Rev.*, 2023, **52**, 3035–3097.

20 J. Chiefari, Y. K. Chong, F. Ercole, J. Krstina, J. Jeffery, T. P. T. Le, R. T. A. Mayadunne, G. F. Meijs, C. L. Moad, G. Moad, E. Rizzardo and S. H. Thang, *Macromolecules*, 1998, **31**, 5559–5562.

21 J. Xu, K. Jung, A. Atme, S. Shanmugam and C. Boyer, *J. Am. Chem. Soc.*, 2014, **136**, 5508–5519.

22 A. R. Kuzmyn and S. de Beer, *Polymer*, 2025, **323**, 128155.

23 A. R. Kuzmyn, M. van Galen, B. van Lagen and H. Zuilhof, *Polym. Chem.*, 2023, **14**, 3357–3363.

24 M. Li, M. Fromel, D. Ranaweera, S. Rocha, C. Boyer and C. W. Pester, *ACS Macro Lett.*, 2019, **8**, 374–380.

25 J. O. Zoppe, N. C. Ataman, P. Mocny, J. Wang, J. Moraes and H.-A. Klok, *Chem. Rev.*, 2017, **117**, 1105–1318.

26 J. Phommalysack-Lovan, Y. Chu, C. Boyer and J. Xu, *Chem. Commun.*, 2018, **54**, 6591–6606.

27 G. Ng, M. Li, J. Yeow, K. Jung, C. W. Pester and C. Boyer, *ACS Appl. Mater. Interfaces*, 2020, **12**, 55243–55254.

28 L.-H. Rong, X. Cheng, J. Ge, O. K. Krebs, J. R. Capadona, E. B. Caldona and R. C. Advincula, *ACS Appl. Polym. Mater.*, 2022, **4**, 6449–6457.

29 B. S. Tucker, M. L. Coughlin, C. A. Figg and B. S. Sumerlin, *ACS Macro Lett.*, 2017, **6**, 452–457.

30 V. Bellotti and R. Simonutti, *Polymers*, 2021, **13**, 1119.

31 S. E. Woods, J. D. Tinkler, N. Bensabeh, M. Palà, S. J. Martin, I. Martin-Fabiani, G. Lligadas and F. L. Hatton, *ACS Sustain. Chem. Eng.*, 2023, **11**, 9979–9988.

32 H. Mori, I. Kato and T. Endo, *Macromolecules*, 2009, **42**, 4985–4992.

33 H. Ma and A. Cameron, *J. Polym. Res.*, 2023, **30**, 278.

34 H. Mori, Y. Ebina, R. Kambara and K. Nakabayashi, *Polym. J.*, 2012, **44**, 550–560.

35 X. Xu, A. E. Smith, S. E. Kirkland and C. L. McCormick, *Macromolecules*, 2008, **41**, 8429–8435.

36 C. M. Schilli, M. Zhang, E. Rizzardo, S. H. Thang, Y. K. Chong, K. Edwards, G. Karlsson and A. H. E. Müller, *Macromolecules*, 2004, **37**, 7861–7866.

37 F. Li, Y. Yu, H. Lv, Y. Wan, X. Gao, Y. Li and Y. Zhang, *Eur. Polym. J.*, 2022, **178**, 111519.

38 M. Kaholek, W.-K. Lee, S.-J. Ahn, H. Ma, K. C. Caster, B. LaMattina and S. Zauscher, *Chem. Mater.*, 2004, **16**, 3688–3696.

39 J. N. Kizhakkedathu, R. Norris-Jones and D. E. Brooks, *Macromolecules*, 2004, **37**, 734–743.

40 X. Sui, S. Zapotoczny, E. M. Benetti, M. Memesa, M. A. Hempenius and G. J. Vancso, *Polym. Chem.*, 2011, **2**, 879–884.

41 A. R. Kuzmyn, A. T. Nguyen, L. W. Teunissen, H. Zuilhof and J. Baggerman, *Langmuir*, 2020, **36**, 4439–4446.

42 A. R. Kuzmyn, L. W. Teunissen, P. Fritz, B. van Lagen, M. M. J. Smulders and H. Zuilhof, *Adv. Mater. Interfaces*, 2022, **9**, 2101784.

43 A. R. Kuzmyn, L. W. Teunissen, M. V. Kroese, J. Kant, S. Venema and H. Zuilhof, *ACS Omega*, 2022, **7**, 38371–38379.

44 B. Hunter, J. L. Sacco, K. Katterle, J. Kirigo, T. K. Wood, E. W. Gomez and C. W. Pester, *Eur. Polym. J.*, 2024, **213**, 113090.

45 G. Ng, P. Judzewitsch, M. Li, C. W. Pester, K. Jung and C. Boyer, *Macromol. Rapid Commun.*, 2021, **42**, 2100106.

46 Q. Hu, W. Wang, T. Ma, C. Zhang, J. Kuang and R. Wang, *Eur. Polym. J.*, 2022, **173**, 111275.

47 P. Skigin, P. Robin, A. Kavand, M. Mensi and S. Gerber-Lemaire, *Polymers*, 2024, **16**, 2873.

48 Q. Ma, W. Wang, L. Zhang and H. Cao, *Macromol. Rapid Commun.*, 2022, **43**, 2200122.

49 J. Poisson, A. M. Polgar, M. Fromel, C. W. Pester and Z. M. Hudson, *Angew. Chem., Int. Ed.*, 2021, **60**, 19988–19996.

50 A. Abbaslı, K. E. Türkmen, D. C. Eren and E. Yildirim, *J. Mater. Chem. B*, 2025, **13**, 8166–8181.

51 A. R. Kuzmyn, T. G. Ypma and H. Zuilhof, *Langmuir*, 2024, **40**, 3354–3359.

52 F. Reyes-Ortega, in *Smart Polymers and Their Applications*, ed. M. R. Aguilar and J. San Román, Woodhead Publishing, 2014, pp. 45–92, DOI: **10.1533/9780857097026.1.45**.

53 R. Hoogenboom, in *Smart Polymers and Their Applications*, ed. M. R. Aguilar and J. San Román, Woodhead Publishing, 2014, pp. 15–44, DOI: **10.1533/9780857097026.1.15**.

54 Y. Yuan, K. Raheja, N. B. Milbrandt, S. Beilharz, S. Tene, S. Oshabaheebwa, U. A. Gurkan, A. C. S. Samia and M. Karayilan, *RSC Appl. Polym.*, 2023, **1**, 158–189.

55 H. Choi, A. Schulte, M. Müller, M. Park, S. Jo and H. Schönherr, *Adv. Healthcare Mater.*, 2021, **10**, 2100069.

56 N. Elmalı, D. Cimen Eren, T. Caykara and E. Yildirim, *Colloids Surf., A*, 2024, **685**, 133335.

57 N. Ejderyan, Y. Oz, R. Sanyal and A. Sanyal, *Biomacromolecules*, 2025, **26**, 1555–1570.

58 L. Zhu, Y. Lu, Y. Wang, L. Zhang and W. Wang, *Appl. Surf. Sci.*, 2012, **258**, 5387–5393.

59 R. A. Zangmeister, T. A. Morris and M. J. Tarlov, *Langmuir*, 2013, **29**, 8619–8628.

60 H. Lee, S. M. Dellatore, W. M. Miller and P. B. Messersmith, *Science*, 2007, **318**, 426–430.

61 E. Zeinali, V. Haddadi-Asl and H. Roghani-Mamaqani, *RSC Adv.*, 2014, **4**, 31428–31442.

62 Merck (Sigma-Aldrich), RAFT: Choosing the Right Agent to Achieve Controlled Polymerization, available at: **https://www.sigmaaldrich.com/TR/en/technical-documents/technical-article/materials-science-and-engineering/polymer-synthesis/raft-polymerization**.

63 E. Yildirim, *Chem. Pap.*, 2020, **74**, 1049–1058.

64 H. Arkaban, M. Barani, M. R. Akbarizadeh, N. Pal Singh Chauhan, S. Jadoun, M. Dehghani Soltani and P. Zarrintaj, *Polymers*, 2022, **14**, 1259.

65 B. N. Dickhaus and R. Priefer, *Colloids Surf., A*, 2016, **488**, 15–19.